JCTC Journal of Chemical Theory and Computation

Atomistic Force Field for Azobenzene Compounds Adapted for QM/MM Simulations with Applications to Liquids and Liquid Crystals

Marcus Böckmann,[†] Christine Peter,*,[‡] Luigi Delle Site,[‡] Nikos L. Doltsinis,*,[†]
Kurt Kremer,[‡] and Dominik Marx[†]

*Lehrstuhl für Theoretische Chemie, Ruhr-Universität Bochum,
44780 Bochum, Germany, and Max-Planck Institut für Polymerforschung,
Ackermannweg 10, 55128 Mainz, Germany*

Abstract: An atomistic force field has been adapted for use in molecular dynamics simulations of molecular materials that contain azobenzene (AB) functional groups. Force field parameters for bonded interactions and partial charges in the AB unit have been derived from ab initio molecular dynamics reference calculations. First applications of the new force field to liquid *trans*- and *cis*-AB are presented, both using a purely classical approach (MM) and a hybrid quantum-classical (QM/MM) simulation scheme. Detailed structural analysis confirms that QM/MM and purely MM simulations yield results that are in good agreement with each other. The force field of the AB core has been extended to include aliphatic chains that are attached via ether bridges to the two AB benzene rings. This allows for studying temperature induced phase transitions in the liquid−crystalline 8AB8 system. Using replica exchange techniques the new force field has successfully reproduced the smectic to isotropic-phase transition.

1. Introduction and Motivation

Azobenzene (AB) has become one of the most widely studied photoactive compounds in physics and chemistry[1–5] mainly because it is possible to reversibly switch between the cis and trans isomers by photoexcitation (see Figure 1a). Although the structure of the electronically excited molecule as well as the mechanism of this photoisomerization still remains an unsolved problem,[6–16] AB is frequently used in practice as an optical switch, for instance to fold/unfold peptides,[17,18] in optomechanical cycles and molecular machines,[19,20] and in developing optically active materials.[1,5,21–29] Most of these applications exploit the large difference of approximately 2.4 Å in the end-to-end distance of the extended trans isomer with respect to the more compact cis isomer. The difference in molecular shape results in crucially different properties. In the field of liquid crystals, for
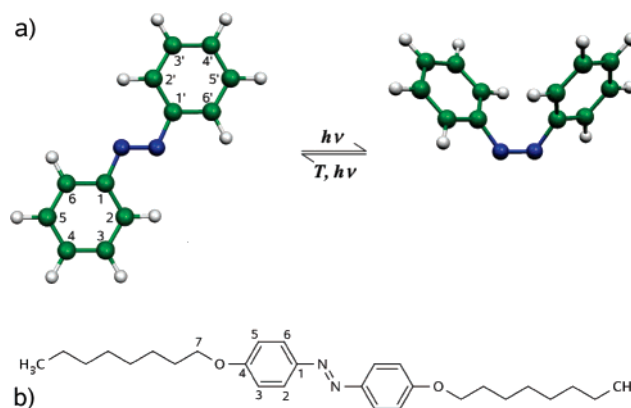

Figure 1. (a) Structure and atom numbering scheme of *trans*- and *cis*-azobenzene in the left and right panels, respectively. (b) Chemical structure of 4,4′-dioctyloxyazobenzene (8AB8).

instance, the stiff, rod-shaped trans isomer of AB can function as a mesogen, occurring in numerous liquid−crystalline compounds, while the nonmesogenic cis isomer is not able to induce any long-range order.[24,30] Hence, it is

* Corresponding author e-mail: peter@mpip-mainz.mpg.de (C.P.)
and nikos.doltsinis@theochem.rub.de (N.L.D.).
† Ruhr-Universität Bochum.
‡ Max-Planck Institut für Polymerforschung.

possible to design AB-containing materials which form photoswitchable liquid crystals.[24,30]

Theoretical modeling of such optically active materials presents a challenge since they are characterized by phenomena that take place on largely different length and time scales: the ultrafast process of photoisomerization, occurring on the (sub-)picosecond time scale, requires the use of state-of-the-art ab initio simulation techniques eventually even going beyond the Born–Oppenheimer approximation, while the macroscopic changes induced by the photoswitching of the AB chromophore, such as phase transitions in liquid crystals, calls for simulation techniques reaching at least into the mesoscopic realm. In the 'hierarchy' of computational methods, going from the atomistic (quantum mechanical: QM) via the microscopic (molecular mechanics: MM) to the mesoscopic (coarse grained: CG) level implies that ab initio molecular dynamics is followed by classical force field molecular dynamics and coarse grained dynamics. A valuable step in between such 'all-QM' and 'all-MM' techniques is the well-known hybrid quantum-classical QM/MM approach, in which only a chemically active subsystem is treated quantum-mechanically (QM), while the remaining part is described by molecular mechanics (MM) employing classical force fields. Unfortunately there is no appropriate force field available that allows for a sound description of the azobenzene functional unit in a macroscopic context.

The strategy we followed in this work was to use a well tested standard force field with a broad range of applications (in this case the GROMOS force field, see below) and to restrict the reparametrization to the photoswitchable azo functional unit, thus retaining the advantages of the well-established standard force field (especially the nonbonded parameters and small charge groups). This implies that we did not aim to develop an optimized (and hence specialized) force field for liquid azobenzene or 8AB8. However, by the same token this means that we retain the universal applicability of the (GROMOS) standard force field. In particular, the standard nonbonded parameters derived from thermodynamic data for various aliphatic and aromatic groups have not been changed in order to ensure this transferability. Furthermore, keeping in mind the aim to treat the photoswitch fully quantum mechanically in a QM/MM framework, its parametrization has been done with reference to the particular QM treatment (in this case the PBE density functional, see below) to be used therein. This allows for a most seemless change between a force field (MM) description and an electronic structure based (QM) description of the photoswitch. These important features of our approach may, for instance, be exploited in future studies of photoswitchable biomolecules.[31]

In the present paper, we attempt to consistently link the most fundamental three hierarchical levels for the specific case of AB itself as well as for AB-containing materials: from QM to QM/MM to MM. The chosen strategy is as follows.

(1) We first carry out finite-temperature ab initio molecular dynamics simulations (all-QM) of *cis-* and *trans-*AB in the gas phase, which will serve as a reference for the MM simulations.

(2) Classical force field simulations (all-MM) of gas-phase AB are performed. Force field parameters for bonded interactions and partial charges in the AB unit are adapted so as to yield maximum agreement between all-QM and all-MM results. In line with our philosophy outlined above, parameters for nonbonded interactions are taken from a well-tested standard force field so as to retain its applicability in a more general context.

(3) The obtained force field is applied to the study of liquid AB using two types of simulation techniques, all-MM and hybrid QM/MM. A detailed comparison in terms of structural parameters is performed.

(4) An extended force field is employed to perform all-MM simulations of an order–disorder-phase transition in the 4,4′-dioctyloxyazobenzene (8AB8)[32] liquid crystal (see Figure 1b). This serves to validate the extended force field by direct comparison with experimental observations.

The above procedure represents the foundation of a genuine multilevel approach to studying optically active materials. In such a scheme, the photoinduced events involving the AB chromophore are treated fully quantum-mechanically, ultimately including even non-Born–Oppenheimer effects, whereas the complex condensed-phase environment, expected to have a considerable impact on the photoisomerization mechanism and efficiency, is described in a QM/MM approximation. Phenomena occurring on much longer (nanosecond) time scales as a result of the initial photoswitching and its picosecond relaxation are modeled using classical MM simulation techniques. It is envisaged to extend further the range of applicability of the present "QM to QM/MM to MM" multiscale ansatz in space and time by introducing both nonadiabatic effects and an additional CG level in the hierarchy which no longer carries atomic resolution but relies on coarse grained interaction potentials. Ultimately, this "QM to nonadiabatic–QM/MM to MM to CG" approach will provide a genuine link between quantum-mechanical events at the level of electrons and nuclei up to the level of macroscopic properties of photo-(re)active materials.

2. Computational Details

2.1. Ab Initio Molecular Dynamics Reference Simulations.
Gas-phase Car–Parrinello ab initio molecular dynamics simulations[33,34] have been performed using the plane wave density functional theory code CPMD.[34,35] We employed the PBE exchange and correlation functional[36,37] and truncated the plane wave expansion of the Kohn–Sham orbitals at 70 Ry and used normconserving pseudopotentials of the Goedecker type for the core electrons. A fictitious electron mass of 800 au and a time step of 5 au (0.12 fs) were chosen replacing as usual the hydrogen mass by the deuterium mass in order to increase the computational efficiency.[34] The size of the periodic simulation cell was $20 \times 13 \times 8$ Å^3 and $17 \times 12.5 \times 12.5$ Å^3 for the isolated *trans-* and *cis-*AB molecules, respectively. The systems were pre-equilibrated for 10 ps at 300 K using a separate Nosé–Hoover chain thermostat[38] for each degree of freedom which ensures very efficient thermalization and energy equipartitioning of even stiff intramolecular rovibrational modes.[39] Based on such

Atomistic Force Field for Azobenzene Compounds

J. Chem. Theory Comput., Vol. 3, No. 5, 2007 **1791**

initial conditions, the systems were left to evolve micro-canonically without the use of any thermostats during the final 12 ps production runs.

In order to determine the barrier height for the torsional cis−trans ground-state isomerization about the N=N bond, which is important for the parametrization of the associated classical force constant, a minimum energy path has been calculated along the CNNC dihedral angle from 0° and 180° in steps of 10°. In addition, ab initio molecular dynamics simulations of methyl phenyl ether ($H_3C-O-C_6H_5$) were carried out at 300 K. This serves as a model system for the ether linkage occurring in AB containing molecules such as 8AB8 (see Figure 1b). A cubic unit cell of length 15 Å was used, whereas the remaining simulation parameters were identical to the AB simulations. After equilibration a production run of 2.4 ps length was performed. In order to determine partial charges, restrained electrostatic potential (RESP) fits[40] were carried out using the CPMD program for constrained optimized geometries at fixed $C^{(5)}C^{(4)}OC^{(7)}$ dihedral angles (see Figure 1 for nomenclature) from 0° to 90° in steps of 10°. The point charges determined for the classical force field have been calculated by Boltzmann averaging over this dihedral angle.

2.2. Classical Gas-Phase Simulations and Force Field Parametrization. A force field suitable for simulations of *trans-* and *cis*-AB was derived starting from the GROMOS 45a3 force field.[41] Using the GROMOS program package,[42,43] we performed MM runs of the isolated trans and cis conformers in the gas phase for 25 ps (after 25 ps of equilibration) using a time step of 1 fs. The temperature was kept constant at 300 K using the Berendsen thermostat[44] with a coupling constant of 0.1 ps. Nonbonded interactions were calculated using a cutoff of 14 Å (updated every 10 steps) (i.e., all nonbonded interactions were taken into account). The parametrization calculations were performed without the use of any bond constraints. Nonstandard force field parameters (i.e., point charges and bonded parameters in the azo group) were determined to achieve maximum compatibility between the QM and MM descriptions. For the bonded parameters this requires that the distributions of bond lengths, bond angles, and dihedral angles obtained from the QM reference simulations are reproduced by the MM force field.

The point charges have been assigned according to the RESP atomic charges as described in section 2.1 from the reference QM calculations on *trans-* and *cis*-AB. In analogy to the force field parametrization procedure for AB, we have developed an extended force field suitable for the 8AB8 compound (see Figure 1b). The required force field parameters for the $C^{(4)}-O-C^{(7)}$ linkage were determined by matching MM and QM simulation data for the methyl phenyl ether ($H_3C-O-C_6H_5$) model system introduced in section 2.1.

2.3. Condensed-Phase Classical Simulations. The purely classical simulations of liquid AB and liquid−crystalline 8AB8 were performed with the Gromacs simulation package.[45] In the case of liquid AB, our simulation box contained 343 such molecules either all in cis or all in trans conformation. The simulations were carried out using a time step of 0.5 fs at a temperature of 400 K and a pressure of 1 bar. A

weak coupling Berendsen algorithm[44] was used to control both temperature (coupling constant: 0.1 ps) and pressure (coupling constant: 5.0 ps, isothermal compressibility: 1.0 × 10⁻⁵ bar⁻¹). Electrostatic interactions were computed using the Particle Mesh Ewald method,[46,47] Lennard-Jones interactions were computed using a cutoff of 20 Å (with pair list updates every 10 steps), and no bond constraints were applied (these settings were also used for the classical part of the QM/MM calculations described below). For the sake of comparison, we also carried out simulations of a single AB molecule where stochastic temperature coupling was used with a friction coefficient of 10 ps⁻¹.

The liquid−crystalline systems contained 1296 8AB8 molecules (four layers of 18 × 18 molecules) prepared in smectic order. Unless stated otherwise, the same computational settings were used as for liquid AB. Here, all chemical bonds were constrained using the LINCS algorithm[48] enabling us to use a time step of 2 fs, and for Lennard-Jones interactions a twin-range cutoff of 10 and 14 Å (updated every 5 steps) was applied.[42] Anisotropic pressure coupling was used, allowing the three box directions to fluctuate independently but keeping the box orthorhombic. After energy minimization and a very short (5 ps) initial relaxation at 300 K with a 0.5 fs time step, the system was equilibrated at 400 K for 800 ps. After equilibration, replica exchange simulations[49] were carried out with seven replicas in a temperature range from 460 to 475 K. This range had been determined by previous simulations at various temperatures between 400 and 500 K such that it covers temperatures where the system remains in the initial layered setup up to temperatures where a transition from the ordered setup to the isotropic phase is observed; the number of replicas is limited due to the required simulation lengths to observe phase changes in the chosen system. Each replica evolved independently, and, after every 4000 MD-steps (∼8 ps), an exchange of pairs of neighboring (in temperature space) replicas was attempted.[49]

For analysis of the liquid−crystalline system, the order parameter S of the system was evaluated, with S being the largest eigenvalue of following tensor

$$Q_{\alpha\beta} = \sum_{j=1}^{N} \left(\frac{3}{2} u_{j\alpha} u_{j\beta} - \frac{1}{2} \delta_{\alpha\beta} \right) \quad \alpha, \beta = x, y, z \qquad (1)$$

where the sum is over all N molecules, the unit vector u_j points along the axis of one molecule or mesogenic unit j (in our case this axis was defined by the positions of the two carbon atoms $C^{(4)}$ and $C^{(4')}$, see Figure 1), and $\delta_{\alpha\beta}$ is the Kronecker delta. For nematic and smectic phases this eigenvalue is significantly larger than the other two indicating the degree of alignment along the direction of the corresponding eigenvector, the so-called director. Thus, the appearance of liquid−crystalline phases can be identified through the order parameter; a distinction of smectic and nematic phase is not possible however. For this, the 3D arrangement of the molecules needs to be analyzed. The smectic phase is characterized by a 2D arrangement of the molecules in (fluid) layers, whereas the nematic phase only exhibits orientational order along the director but no positional order.

2.4. QM/MM Simulations. The hybrid QM/MM simulations of liquid AB were carried out using the CPMD/GROMOS interface[50] developed by Laio et al. that couples the Car−Parrinello molecular dynamics package CPMD[34,35] to the GROMOS molecular dynamics package[42,43] (see ref 51 for a review). Within this coupling scheme a single QM AB molecule was immersed in a liquid consisting of MM AB molecules. The electronic structure treatment of the QM subsystem is identical to that described in section 2.1 for isolated AB molecules, while the classical force field (see sections 2.2 and 2.3) is used to describe the MM subsystem.

Starting from an equilibrated configuration obtained from a purely classical (MM) simulation of 343 *trans*-AB molecules in a cubic box of length 45.2 Å (the average from the constant pressure MM simulation described in section 2.3), a hybrid QM/MM simulation was performed at 400 K using Nosé−Hoover chains[38] for both ions and electrons and a time step of 5 au (0.12 fs). The length of the production run was about 3 ps. The center-of-mass translation and overall rotation was removed every 10 time steps.

A single AB molecule was treated quantum-mechanically in a cubic box of length 18 Å for both *trans*- and *cis*-AB. QM atoms carry the same nonbonded parameters as the MM atoms. The cutoff for the explicit interaction of the remaining MM atoms with the QM charge density, i.e., the nearest-neighbor cutoff, between the charge group centers was set to 20.0 au (10.6 Å), and the nearest-neighbor list was updated every 10 time steps. Charge groups at distances greater than 20.0 au interact with the QM subsystem through a multipole expansion of the QM charge density. In order to prevent the QM subsystem from artificial cooling as often observed in QM/MM calculations we applied two separate Nosé−Hoover chains[38] to the QM and MM subsystems.

3. Results and Discussion

3.1. Ab Initio Simulations of Azobenzene in the Gas Phase. As a basis for the AB force field parametrization, we performed two separate ground-state Car−Parrinello simulations of an isolated *trans*- and *cis*-AB molecule at 300 K. In the following discussion, the focus is on internal coordinates involving the azo group (see Figure 1 for structure and numbering), that is, the NN′ and $C^{(1)}N$ bond lengths (the latter being equivalent to the $C^{(1')}N'$ bond length due to the molecular symmetry), the $C^{(1)}NN'$ (and also $C^{(1')}N'N$) bond angle, the $C^{(1)}NN'C^{(1')}$ dihedral angle, and the rotation of the two aromatic ring systems described by the dihedral angles $\Phi_1 = \angle C^{(2)}C^{(1)}NN'$ and $\Phi_2 = \angle C^{(2')}C^{(1')}N'N$. As a measure for pyramidalization at $C^{(1)}$ we chose the angle between the $C^{(1)}N$ bond and the $C^{(6)}C^{(1)}C^{(2)}$ plane which is the so-called Wilson angle.[52] In the following we omit the atomic indices and refer to the CN bond length, the CNN bond angle, and the CNNC dihedral angle for simplicity.

Figure 2 depicts the time evolution of the CNNC dihedral, the ring rotational angles Φ_1 and Φ_2, and the pyramidalization at $C^{(1)}$, in the case of the *trans*-AB conformer. The upper panel of Figure 2 illustrates that the molecule is planar on average, the CNNC dihedral exhibiting rather regular oscillations about 180° with an amplitude of roughly 20°. The middle panel of Figure 2 demonstrates that the rotational
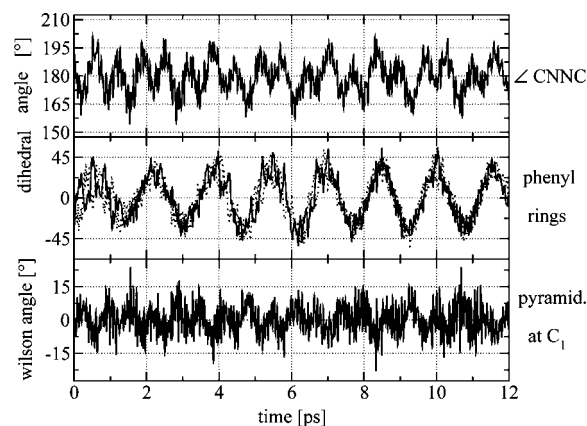

Figure 2. Time evolution of structural parameters from an ab initio molecular dynamics simulation of isolated *trans*-AB at 300 K. Top panel: dihedral angle CNNC. Middle panel: rotation angles Φ_1 and Φ_2 for the two phenyl rings (solid and dotted lines). Bottom panel: pyramidalization angle (see text) at the carbon atom $C^{(1)}$.

motion of the phenyl rings is concerted for *trans*-AB. Each individual phenyl ring rotates up to $\Phi_{1,2} \approx \pm 30°$, while maintaining $\Phi_1 \approx \Phi_2$ throughout. In other words, given the definition of Φ_1 and Φ_2, the two phenyl rings are found to rotate against each other ('out-of-phase'), resulting in an overall (approximate) C_2 symmetry of *trans*-AB.

If the rotation were 'in-phase', i.e. $\Phi_1 = -\Phi_2$, the molecular symmetry would be C_i (assuming planarity and equal bond lengths in both aromatic rings). The question of whether vibrational motion in AB leads to C_2 or C_i symmetry has been controversially debated in the literature.[53,54] Our current results are in line with the experimental findings from gas-phase electron diffraction studies by Adamson et al.[53] suggesting C_2 symmetry. As can be seen from the bottom panel of Figure 2, there is no pyramidalization at $C^{(1)}$ on average, but fluctuations of $\approx \pm 15°$ are observed; this observation holds for $C^{(1')}$, too.

It is revealing to compare the dynamics of *trans*-AB (Figure 2) to that of its *cis*-AB analogue shown in Figure 3. In the case of *cis*-AB, the central CNNC unit is nonplanar on average, the CNNC dihedral being $-10 \pm 20°$ (Figure 3, upper panel). Furthermore, the CNNC dihedral oscillations are seen to have a much higher frequency compared to *trans*-AB. In addition, in order to minimize steric interactions, the phenyl rings are rotated by $\Phi_{1,2} = -52 \pm 17°$ as seen from the middle panel. The events where Φ_1 gets close to zero while Φ_2 is close to $-90°$ can be viewed as attempted ring flips. In contrast to the trans conformer, a substantial amount ($\approx 8°$) of pyramidalization is observed for the $C^{(1)}$ carbon atom connected to the nitrogens (Figure 3, bottom panel); the same amount of pyramidalization is found for $C^{(1')}$.

The average values for selected structural parameters from these ab initio molecular dynamics gas-phase runs are collected in Table 1 together with our results from structure optimizations as well as published quantum chemical and experimental data. As expected, for the (nonplanar) cis conformation the NN′ bond distance is shortened, and the CN bond distance is elongated compared to the trans conformation. The steric hindrance of the aromatic ring

Atomistic Force Field for Azobenzene Compounds

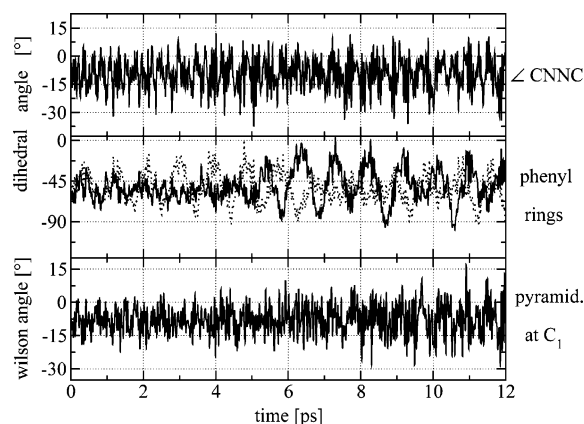*J. Chem. Theory Comput., Vol. 3, No. 5, 2007* **1793**

Figure 3. Time evolution of structural parameters from an ab initio molecular dynamics simulation of isolated *cis*-AB at 300 K. Top panel: dihedral angle CNNC. Middle panel: rotation angle Φ_1 and Φ_2 for the two phenyl rings (solid and dotted lines). Bottom panel: pyramidalization angle (see text) at the carbon atom $C^{(1)}$.

systems in the cis conformation results in a CNNC dihedral angle of 9.6° (optimized structure) and, in addition, a significantly (by ≈5−10°) increased CNN bond angle. Comparing the average structures to the optimized structures it is interesting to note that our simulations suggest a shortening of the NN bond and a lengthening of the CN bond at finite temperature in the trans case, while the opposite trend is observed for the cis isomer.

Importantly, the overall agreement of our structures and relative energetics for the optimized structures in comparison to experimental data and quantum chemical calculations is good. Thus, the electronic structure approach chosen and the generated ab initio trajectories can be considered as accurate reference data in order to parametrize a classical force field.

3.2. Force Field Parametrization. Using the GROMOS 45a3 force field as a starting point to derive a new force field suitable for AB, we adjusted only the bonded parameters and the charges of the azo group while keeping the original values for the remaining parameters. The parametrization was carried out in such a way as to achieve maximum agreement between the dynamical distributions obtained from force field and ab initio molecular dynamics simulations in the gas phase at 300 K concerning the relevant bond lengths, bond angles, and dihedral angles. This will ensure maximum compatibility between the QM and MM descriptions—so that switching adaptively between the quantum-mechanical (atomistic) and classical (microscopic) description for a given AB unit is as smooth as possible in future adaptive applications. Table 2 summarizes our results for the nonstandard parameters. In all cases, the values for the force constants are adapted to reproduce the widths of the distributions of bond lengths, angle, and dihedrals, starting out from the force field's standard values for chemically similar internal coordinates. In this spirit, we also decided to use the same force constants and point charges for the cis and trans isomers; only the equilibrium reference values for the bonded potentials differ.

The point charges for the atoms $C^{(1)}$ and N were adapted from average RESP charges[55] computed along the ab initio molecular dynamics reference trajectories. Since the values

obtained for the aromatic ring atoms $C^{(2)}-C^{(6)}$ and the hydrogen atoms were close to their standard force field values, we decided to use the standard values and thus to take advantage of the resulting small charge groups. Note that in contrast to the GROMOS convention but in line with the AMBER convention[56] and in order to distribute the forces evenly over all contributing atoms we define explicitly *all* dihedral angles involving the two CN bonds, i.e., the dihedral angles $C^{(6)}C^{(1)}NN'$, $C^{(2)}C^{(1)}NN'$, $C^{(6')}C^{(1')}N'N$, and $C^{(2')}C^{(1')}N'N$, which consequently results in smaller force constants per dihedral compared to standard force field values.

The resulting distributions obtained with our new, separate cis and trans force fields are presented in Figure 4 together with the ab initio molecular dynamics results. Note that using different parameters for *trans*- and *cis*-AB, the distributions obtained from the ab initio molecular dynamics runs can be reproduced very accurately. However, it is our aim here to derive a single, unified force field which can be applied to study, for instance, a mixture of *trans*- and *cis*-AB molecules in the condensed phase. In addition, such a force field does not need to be modified during a simulation once a photoinduced cis/trans conformational change (or vice versa) has occurred in future nonadiabatic QM/MM simulations. Therefore, in the applications described below, we employ the average values given in the last column of Table 2.

The most striking deviation between the force field and reference data occurs for the dihedral angle ∠CNNC (fourth row in Figure 4). Note that the force constant associated with this degree of freedom not only influences the broadness of the thermal distribution observed in a molecular dynamics run but also, more importantly, governs the barrier height for the thermal trans/cis isomerization in the ground state. Based on recent ab initio calculations[8] this barrier is predicted to be ≈160 kJ/mol (see Table 1), and the new force field yields a barrier along the torsional reaction coordinate of ≈140 kJ/mol. Increasing the barrier in the force field would yield to an even narrower distribution function for the dihedral CNNC angles. On the other hand, the presently parametrized barrier height is sufficiently large to prevent thermally induced cis/trans isomerizations in the simulations of bulk AB at 400 K (see section 3.3), which should not occur on the time scale accessible to classical simulation.

In Table 1 the resulting data for the optimized structures (see 'MM (trans)' and 'MM (cis)' entries) as well as those for the unified, average force field (see 'MM (average)' entries) are collected together with our static and dynamic QM reference results (see 'DFT/PBE' and 'DFT/PBE (300 K)' entries, respectively) and compared to the literature. The data again underline the good quality of our parameter set for *trans*- and *cis*-AB, respectively. However, it becomes obvious that using the average values (for the sake of methodological consistency and ease) instead of the separate cis and trans parameters leads necessarily to some systematic deviations concerning the bond angle and, more pronounced, the bond lengths.

Based on this force field for the AB chromophore we have extended the set of force field parameters to be able to study materials containing this photoswitch such as 8AB8 introduced in Figure 1 where aliphatic side chains are attached

Table 1. Comparison of Structures and Relative Energies of an Isolated Azobenzene Molecule[a]

	method	E_{rel}	r_{NN}	r_{CN}	∠CNN	∠CNNC
	trans-AB					
literature:	CASSCF(14,12)/6-31G* [8]	0.0	1.243	1.422	115.1	180.0
	MP2/cc-pVTZ[60]	-	1.268	1.417	113.7	180.0
	DFT/BP86/TZVP[60]	-	1.267	1.420	114.8	180.0
	semiemp AM1 (mod)[12]	0.0	1.239	-	117.5	180.0
	exp. (X-ray)[61]	-	1.247	1.428	114.1	180.0
	exp. (electr diffr)[62]	-	1.25	1.43	114.1	180.0
this work:	DFT/PBE	0.0	1.270	1.426	114.6	180.0
	DFT/PBE (300 K)	-	1.263	1.450	114.5	180.0
	MM(trans)	-	1.269	1.428	115.8	180.0
	MM(average)	-	1.261	1.435	118.0	180.0
	cis-AB					
literature:	CASSCF(14,12)/6-31G* [8]	68.5	1.242	1.435	122.9	4.2
	CASPT2(14,12)/6-31G* [8]	50.2	1.242	1.435	122.9	4.2
	MP2/cc-pVTZ[60]	-	1.261	1.432	120.8	7.3
	DFT/BP86/TZVP[60]	-	1.255	1.437	124.1	11.4
	semiemp AM1 (mod)[12]	38.6	1.221	-	124.3	4.1
	exp. (X-ray)[63]	-	1.253	1.449	121.9	8.0
	exp. (ΔH)[64]	56.0	-	-	-	-
	exp. (ΔH)[53]	50.3	-	-	-	-
this work:	DFT/PBE	58.3	1.261	1.442	123.6	9.6
	DFT/PBE (300 K)	-	1.277	1.430	124.5	7.5
	MM(cis)	-	1.260	1.444	125.1	5.7
	MM(average)	-	1.266	1.435	122.6	5.4
	AB Transition State					
literature:	CASSCF(14,12)/6-31G* [8]	173.7	1.304	1.370	122.2	85.3
	CASPT2(14,12)/6-31G* [8]	159.2	1.304	1.370	122.2	85.3
	semiemp AM1 (mod)[12]	193.0	1.244	-	129.5	90.0
this work:	DFT/PBE	169.9	1.290	1.364	125.2	89.4
	MM(average)	137.6	1.269	1.427	115.2	90.0

[a] Relative energies, E_{rel}, are given in kJ/mol, bond lengths in Å, and angles in degrees. The DGT/PBE (300 K) data are average values obtained from the ab initio molecular dynamics trajectories (see text). The MM data are from optimized geometries using separate force fields for cis and trans and the unified *average* force field, respectively.

Table 2. Nonstandard Force Field Parameters Derived for Azobenzene[a]

	entity		force constant	reference value		
				trans	cis	average
bonds:	NN		1.40×10^3 kJ/(mol Å⁴)	1.270 Å	1.255 Å	1.2625 Å
	CN		0.72×10^3 kJ/(mol Å⁴)	1.425 Å	1.440 Å	1.4325 Å
angles:	CNN		650.0 kJ/mol	114.0°	119.0°	116.5°
	CCN		560.0 kJ/mol	120.0°	120.0°	120.0°
dihedrals:	CNNC		70.0 kJ/mol	180°	180°	180°
	CCNN		6.0 kJ/mol	180°	180°	180°
	XCCX		40.0 kJ/mol	180°	180°	180°
point charges:	N			−0.200 *e*	−0.200 *e*	−0.200 *e*
	$C^{(1)}$			0.200 *e*	0.200 *e*	0.200 *e*
	$C^{(2)}-C^{(6)}$			−0.100 *e*	−0.100 *e*	−0.100 *e*
	H			0.100 *e*	0.100 *e*	0.100 *e*

[a] For azobenzene structure and atomic numbering scheme see Figure 1a (X denotes *any* atom).

to the phenyl rings of AB via ether bridges. We used methyl phenyl ether ($H_3C-O-C_6H_5$) as a model system to derive the force field parameters necessary to describe the $C^{(4)}-O-C^{(7)}$ link unit (see Figure 1 for atomic numbering scheme), whereas the remainder of these side chains will be treated using standard force field parameters.

As for AB itself a Car–Parrinello run at 300 K was performed with $HH_3C-O-C_6H_5$ as QM reference with the aim to parametrize those internal coordinates that involve the oxygen atom of the ether group. In order to take into account dynamical fluctuations of the $C^{(5)}C^{(4)}OC^{(7)}$ dihedral angle, RESP charges for $C^{(4)}$, O, and $C^{(7)}$ were calculated for different angles between 0° and 90° in steps of 10°. The resulting charge of the methyl group is taken as the charge of the alkyl carbon atom $C^{(7)}$ (united atom approach), and the resulting charge of the aryl carbon atom $C^{(4)}$ is adjusted so as to yield a neutral $C^{(4)}-O-C^{(7)}$ unit. Force field point charges were then obtained by Boltzmann averaging over

Atomistic Force Field for Azobenzene Compounds

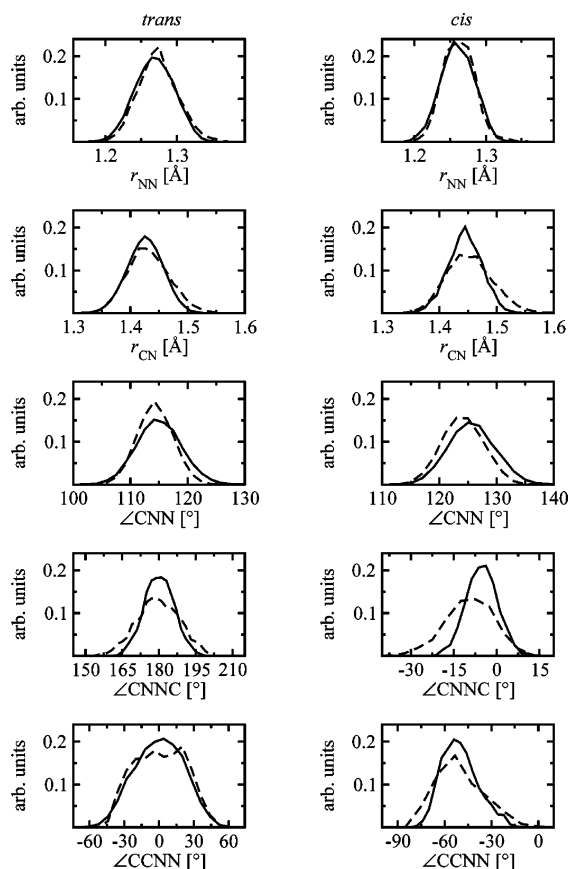*J. Chem. Theory Comput., Vol. 3, No. 5, 2007* **1795**

Figure 4. Structural analysis for classical force field (solid lines) and ab initio (dashed lines) molecular dynamics simulations of *trans-* (left panels) and *cis-* (right panels) AB at 300 K in terms of distribution functions for selected internal coordinates. The classical distributions were obtained from two separate force field parametrizations for cis and trans.

Table 3. Extension of Azobenzene Force Field To Include Ether Linkage $C^{(4)}-O-C^{(7)}$ [a]

	entity	force constant	ref value
bonds:	$OC^{(7)}$	8.18×10^2 kJ/(mol Å⁴)	1.430 Å
	$C^{(4)}O$	1.02×10^3 kJ/(mol Å⁴)	1.360 Å
angle:	$C^{(4)}OC^{(7)}$	620.0 kJ/mol	116.0°
dihedral:	$C^{(3,5)}C^{(4)}OC^{(7)}$	6.0 kJ/mol	180°
point charges:	O		−0.332 *e*
	$C^{(7)}$		0.178 *e*
	$C^{(4)}$		0.154 *e*

[a] See Figure 1 for structure and atomic numbering scheme.

the torsion−angle dependent RESP charges. The resulting parameters for the ether linkage are collected in Table 3.

3.3. Classical Simulation of Liquid Azobenzene. Parametrizations of the azo group had been carried out at 300 K having in mind future applications of the force field at ambient conditions. The present applications to the study of liquid AB (with a melting point of 341 K) and liquid−crystalline AB-containing compounds (with phase transition temperatures of 8AB8 between 372 and 385 K) required testing the validity of the classical force field at an increased temperature of 400 K.

In the following we apply the new force field to study liquid AB at 400 K and analyze separately the influence of
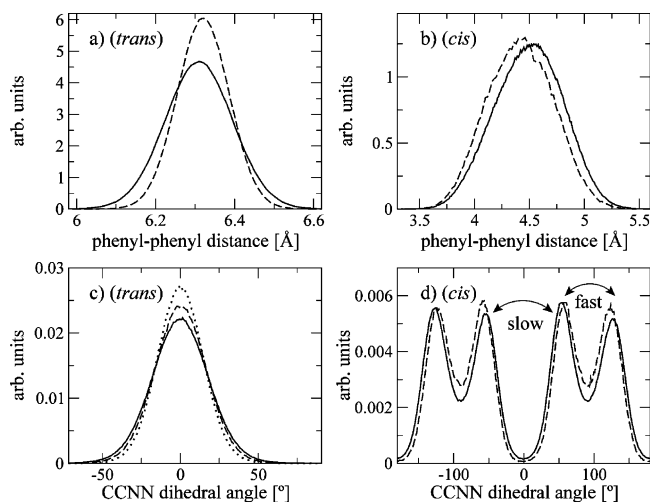

Figure 5. Distributions of structural parameters of the AB unit under various conditions at 400 K. Panels a and b: distance of the geometrical centers of the two phenyl rings. Panels c and d: CCNN dihedral angle. Panel a: *trans*-AB in liquid phase as well as in vacuum − solid line, *trans*-8AB8 in liquid phase (both isotropic and smectic) and in vacuum − dashed line; panel b: *cis*-AB in liquid phase − solid line, *cis*-AB in vacuum − dashed line; panel c: *trans*-AB in liquid phase (equivalent to *trans*-AB in vacuum and *trans*-8AB8 in vacuum) − solid line, *trans*-8AB8 in isotropic liquid − dashed line, *trans*-8AB8 in anisotropic (smectic) phase − dotted line; panel d: *cis*-AB in liquid phase − solid line, *cis*-AB in vacuum − dashed line.

the liquid environment on the structural properties of the cis and trans conformers of AB by comparison with gas-phase simulations at 400 K. As a measure for the extension of the AB unit serves the distribution of the distance between the geometric centers of the two phenyl rings as shown in Figure 5a,b. For *trans*-AB the distributions of the single molecule and the liquid phase are indistinguishable (solid line in Figure 5a), whereas the conformations of the cis isomer are slightly more affected by the bulk environment (see Figure 5b). In the liquid phase the *cis*-AB unit is slightly stretched out compared to the vacuum simulations. Similar observations can be made when analyzing the out-of-plane motions of the phenyl rings by monitoring the distribution functions of the dihedral angle between the normal vectors of the two phenyl rings (data not shown) and of the CCNN dihedral angle (see Figure 5c,d). The conformations in *trans*-AB are not affected by the liquid environment (solid line in Figure 5c), whereas in the case of the cis conformer the amplitude of the ring motion (compared to a planar structure) is slightly larger in the isolated molecule than in the bulk liquid at the same temperature (see Figure 5d). Additionally, it was found that the distribution functions of the CNNC dihedral angle are not affected by the liquid environment—neither in the case of the trans nor in the case of the cis isomer (data not shown), and it was tested that the system does not undergo thermal cis/trans isomerization, which is a rare event that indeed should not occur on the time scale presently accessible by such classical molecular dynamics simulations.

Figure 5d shows that the distribution of the CCNN dihedral angle in *cis*-AB has four chemically equivalent maxima
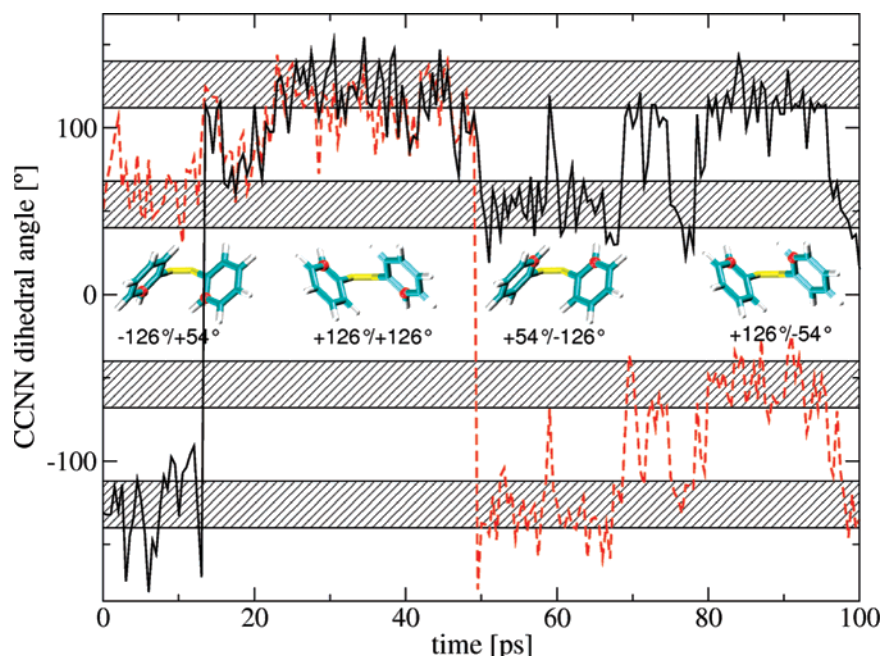
Figure 6. Time evolution of the CCNN dihedral angles of a *cis*-AB molecule in liquid environment at 400 K. The striped bars indicate the regions ($\pm14°$ around the maxima of the distributions at $\pm54°$ and $\pm126°$, see Figure 5d) used to count the transitions between the states (see text). Snapshots of typical conformations are included with the $C^{(2)}$ and $C^{(2')}$ carbon atoms that are used to define the CCNN dihedral angles marked in red.

around $\pm54°$ and $\pm126°$ and consequently two types of transitions between these states. As indicated in the figure, there is one "fast" type of transition, where the phenyl ring is intermediately standing perpendicular to the plane spanned by the $C^{(1)}$ (or the $C^{(1')}$) carbon and the two N atoms, and one "slow" type of transition, where the ring is intermediately in-plane with the $C^{(1)}$ and the two N atoms (to avoid steric hindrance in this planar conformation during the "slow" transition, the second phenyl ring has to "make way" by adopting a conformation perpendicular to the plane). These transitions are observed in the classical simulations of *cis*-AB, whereas the time scale of QM simulations of a few ps are too short to sample these transitions systematically. Figure 6 shows one example of such a process by monitoring the dynamics of the CCNN dihedral angles of one AB unit in a simulation of liquid *cis*-AB at 400 K, where both types of transitions are observed. In addition, snapshots of representative *cis*-AB conformations are shown to illustrate the conformational changes during the transitions. In order to get a rough estimate for the time scale of these ring flips the transitions of both types are counted for all CCNN dihedrals in a simulation of 343 *cis*-AB molecules at 400 K. Since the separation between the states, in particular between the states involved in the "fast" transitions, is ambiguous, narrow regions ($\pm14°$) around the maxima of the distributions at $\pm54°$ and $\pm126°$ were defined (as marked in Figure 6), and only transitions between these regions were counted. This results in transition times of approximately 20 ps for the "fast" and 200 ps for the "slow" ring flips. By Boltzmann inverting the dihedral distribution in Figure 5d, one obtains an effective barrier for the "fast" transition of the order of about 3 kJ/mol ($\approx 1\ k_BT$, where k_B is the Boltzmann constant) and for the "slow" transition a barrier of about 12 kJ/mol ($\approx 4\ k_BT$), which approximately reproduces the relative

magnitude of the two transition rates extracted from the dynamics.

3.4. Hybrid QM/MM Simulations of Bulk Liquid Azobenzene. Using the hybrid CPMD/GROMOS interface[50,51] we performed two QM/MM Car–Parrinello simulations of liquid AB consisting of 343 *cis*- and *trans*-AB molecules each as described in more technical detail in section 2.4. Therein, only a single AB molecule is treated quantum-mechanically (QM AB) and interacts via the interface with the remaining 342 AB molecules which themselves interact with each other according to the molecular mechanics force field (MM AB) generated in section 3.2.

For liquid *trans*-AB, Figure 7 shows the dihedral CNNC angle, the rotation angles Φ_1 and Φ_2 of the two phenyl rings, and the pyramidalization at the $C^{(1)}$ and $C^{(1')}$ carbon atoms of the QM AB molecule (compare to Figure 2 for the corresponding gas-phase results). In contrast to the gas phase, the two aromatic ring systems now move in a C_i-like fashion ($\Phi_1 \approx -\Phi_2$) in the condensed phase, and thus the relative orientation of the two aromatic ring systems is much more conserved in the bulk liquid (compare to Figure 7, center panel). This suggests that in the liquid phase the aromatic ring systems are more or less "pinned' by the neighboring molecules, and the change in the dihedral angles Φ_1 and Φ_2 is mainly due to the mobility of the central nitrogen atoms.

In order to prove that the division of the QM/MM system into 'near' and 'far' coupling regions (see section 2.4) produces a homogeneous description of the liquid phase, we analyzed the structural distributions in these different regions.

Note that the 'near' ABs (center-of-mass distance < 20 au) interact directly with the charge density of the quantum AB molecule, while the 'far' ABs (center-of-mass distance > 30 au) interact through the multipole expansion.

Atomistic Force Field for Azobenzene Compounds

J. Chem. Theory Comput., Vol. 3, No. 5, 2007 **1797**
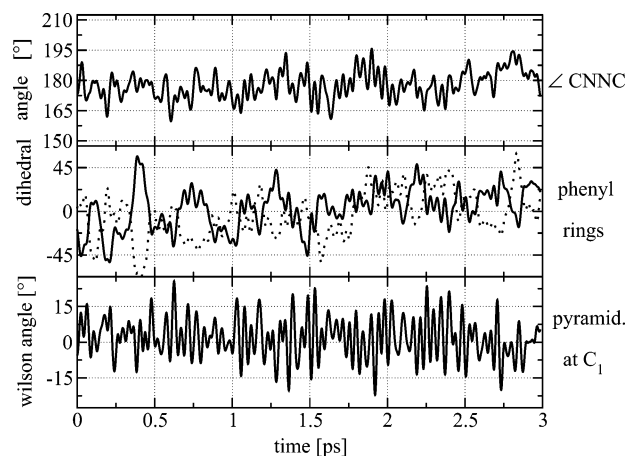

Figure 7. Time evolution of structural parameters of the QM AB unit in bulk liquid *trans*-AB from a QM/MM simulation at 400 K. Top panel: dihedral angle CNNC. Center panel: rotation angle Φ_1 and Φ_2 for the two aromatic rings (solid and dotted lines). Bottom panel: pyramidalization angle (see text) at the carbon atom $C^{(1)}$.
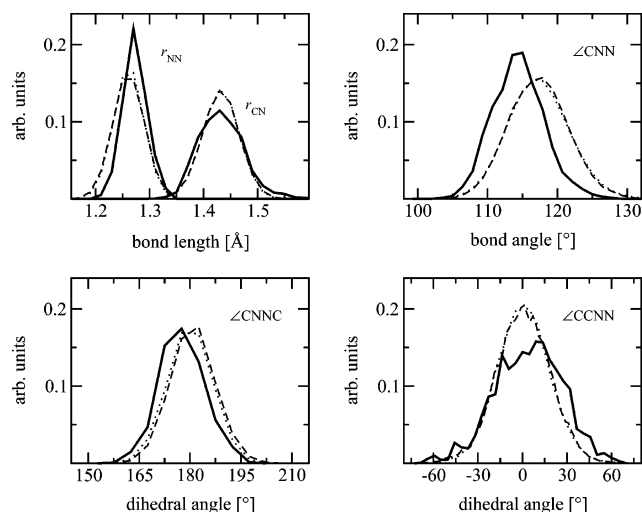

Figure 8. Distributions of selected internal coordinates from a QM/MM simulation of bulk liquid *trans*-AB at 400 K: QM AB (solid lines), near (center-of-mass distance $R < 20$ au) MM molecules (dashed lines), far ($R > 30$ au) MM molecules (dotted lines).

The resulting distribution functions for the QM AB, the 'near' ABs, and the 'far' ABs of the structural parameters of the CNNC group are given in Figure 8. For the 'near' and 'far' MM ABs, the curves are almost identical (dashed and dotted lines, respectively). This demonstrates that the QM/MM coupling scheme applied indeed results in homogeneous properties of the liquid azobenzene system.

In addition, the distributions for the QM AB molecule show the same broadness, but they appear to be slightly but systematically shifted as made most evident by the CNN bond angle distribution. This shift is due to the fact that in the force field description we use for reasons explained earlier the average reference values from Table 2 (see Figure 4) instead of the specific parametrizations for the *cis*- and *trans*-AB conformers which are also available. We would like to point out, however, that the statistical uncertainty in the
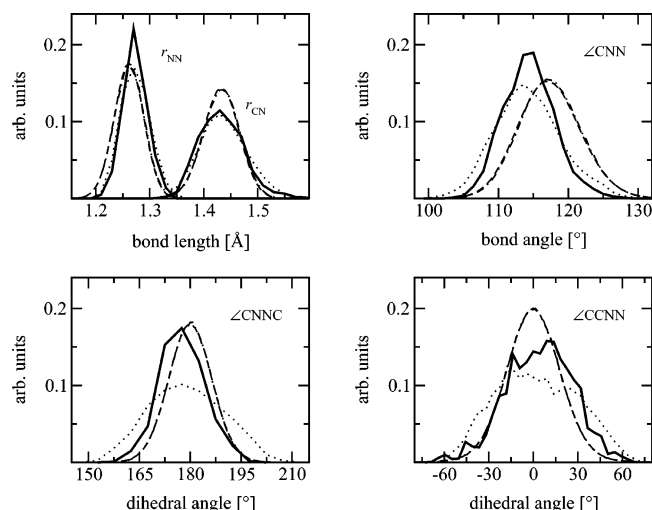

Figure 9. Comparison of selected internal coordinates from the QM/MM simulation (QM molecule, solid lines) of bulk liquid *trans*-AB at 400 K to all-MM bulk (dashed lines), QM gas-phase (dotted lines), and MM gas-phase (dashed-dotted lines) simulations.

distributions for the QM molecule is of course much larger than for the ensemble-averaged MM distributions, which must be considered when comparing the QM distribution to the two MM distributions in Figure 4.

A comparison of the distribution functions of structural parameters for the QM AB molecule in the QM/MM simulation with purely classical simulation data of all-MM liquid AB is shown in Figure 9. The difference between the QM/MM and the all-MM data is comparable to the difference between the QM and MM subsystems within the QM/MM simulation itself (see Figure 8). Furthermore, Figure 9 shows a comparison of bulk distribution functions with those in the gas phase. In particular the CNNC dihedral angle distribution is seen to be much more confined in the liquid-state environment.

The time evolution of different structural variables from the QM/MM simulation of liquid *cis*-AB can be analyzed with the help of Figure 10 (to be compared with Figure 7 for the situation with only *trans*-AB molecules in the liquid). The top panel depicts the rotational motion about the N=N double bond; the corresponding CNNC dihedral angle is found to fluctuate about 12° by ±15° flipping twice into a symmetrically equivalent position with a negative value of the CNNC dihedral angle at about 0.9 and 1.7 ps. As such a flip is not observed for the gas-phase trajectory (see Figure 3), this may be due to solvation effects of the neighboring MM AB molecules. The rotational motion of the two phenyl rings is seen to be much more hindered (see Figure 10: middle panel) than in the gas phase (see Figure 3), since the CCNN dihedral angle is only about 45° and the fluctuations are less pronounced. At about 1.7 ps and coinciding with the second flip of the CNNC dihedral angle (see above), the relative orientation of the two phenyl rings (see Figure 3: middle panel, solid line) approaches 90°, with one ring roughly perpendicular and the other one roughly parallel to an idealized CNNC plane. This may be viewed as an (unsuccessful) ring flip scenario similar to those described
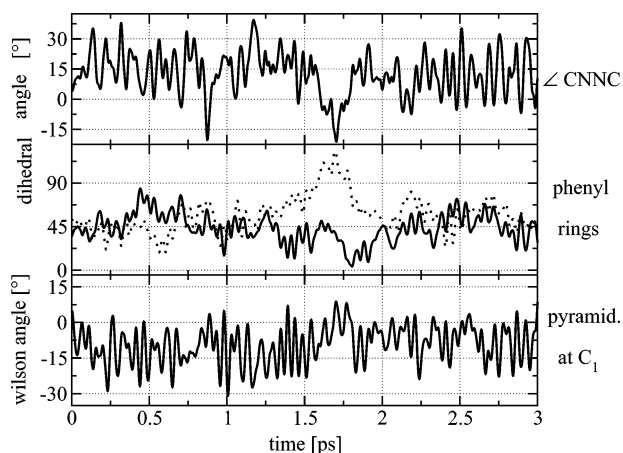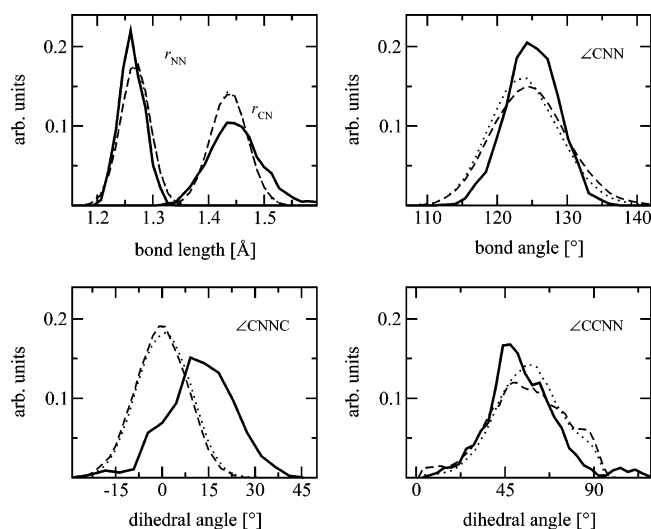
Figure 10. Time evolution of structural parameters of the QM AB unit in bulk liquid *cis*-AB from a QM/MM simulation at 400 K. Top panel: dihedral angle CNNC. Center panel: rotation angle Φ_1 and Φ_2 for the two aromatic rings (solid and dotted lines). Bottom panel: pyramidalization angle (see text) at the carbon atom $C^{(1)}$.

Figure 11. Distributions of selected internal coordinates from a QM/MM simulation of bulk liquid *cis*-AB at 400 K: QM AB (solid lines), near (center-of-mass distance $R < 20$ au) MM molecules (dashed lines), far ($R > 30$ au) MM molecules (dotted lines).

for the all-MM calculation (see section 3.3). The bottom panel of Figure 10 shows that the average pyramidalization of the carbon atom $C^{(1)}$ ($C^{(1')}$ behaves analogously) is as pronounced as in the gas phase (see Figure 3), however exhibiting even larger fluctuations.

Like in the *trans*-AB case, Figure 11 presents histograms of structural parameters from the *cis* QM/MM simulation divided into contributions from the QM molecule itself as well as the near (center-of-mass distance $R < 20$ au) and far ($R > 30$ au) MM solvent molecules. As for the liquid *trans*-AB, there is little difference between near and far MM AB molecules, and the distributions for the QM AB molecule again show the same broadness. In case of the CNNC dihedral angle, there is a significant shift due to the fact that the reference value of the force field corresponds to 0°. The CCNN dihedral angle distributions for the different regions
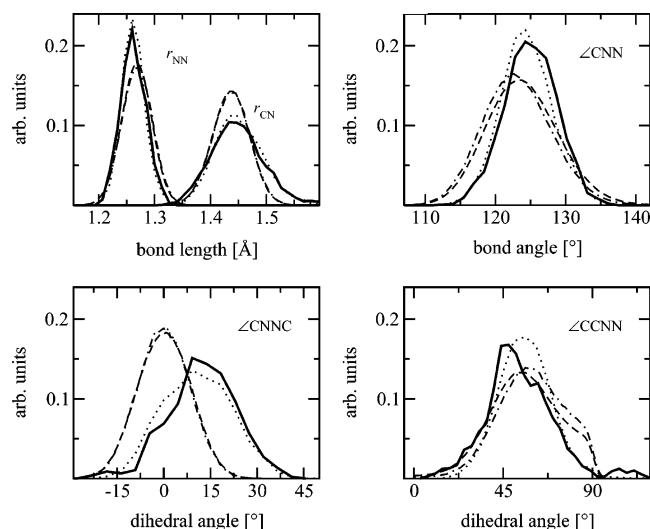

Figure 12. Comparison of selected internal coordinates from the QM/MM simulation (QM molecule, solid lines) of bulk liquid *cis*-AB at 400 K to all-MM bulk (dashed lines), QM gas-phase (dotted lines), and MM gas-phase (dashed-dotted lines) simulations.

are in good agreement with each other. For the ease of comparison the four peaks visible in Figure 5d have been mapped onto the ±54° region.

Figure 12 compares the structural distribution functions from the liquid *cis*-AB QM/MM simulation to all-MM simulations of liquid AB, on the one hand, and to gas-phase all-QM and all-MM data, on the other hand. In particular, when comparing all-QM gas-phase data to the QM subsystem in QM/MM simulations, one notices a slight smearing out of the histograms in solution. Deviations between the liquid-phase QM/MM and MM distributions are similar to those observed in Figure 11 between the QM and MM subsystems in the QM/MM simulation.

3.5. Classical Simulations of the 8AB8 Liquid Crystal. In this section, we present the application of the azobenzene force field to the liquid−crystalline-phase behavior of 8AB8 (sketched in Figure 1b). This AB containing liquid crystal exhibits in experiments a crystalline → nematic-phase transition at 372 K followed by a nematic → isotropic-phase transition at 385 K; in addition there is a monotropic nematic → smectic C-phase transition at 368 K upon cooling. The main intention here is to explore the phase behavior of 8AB8 using classical atomistic (MM) simulations. The stimulation for doing so is 2-fold. First of all, we want to lay the foundation for future QM/MM studies on the photoisomerization of azobenzene compounds in bulk liquid and the anisotropic liquid−crystalline environments and, second, for the development of a coarse grained model of 8AB8 to investigate the photoinduced-phase transition itself. It should be noted that this section does not primarily serve as a test of the quality of the force field as explained in the Introduction.

A system of 1296 8AB8 molecules was setup initially in a smectic arrangement (i.e., the starting structure consisted of four 8AB8 layers of 324 molecules each in an ortho-rhombic box). In order to investigate the phase behavior of the system, replica exchange simulations in a temperature
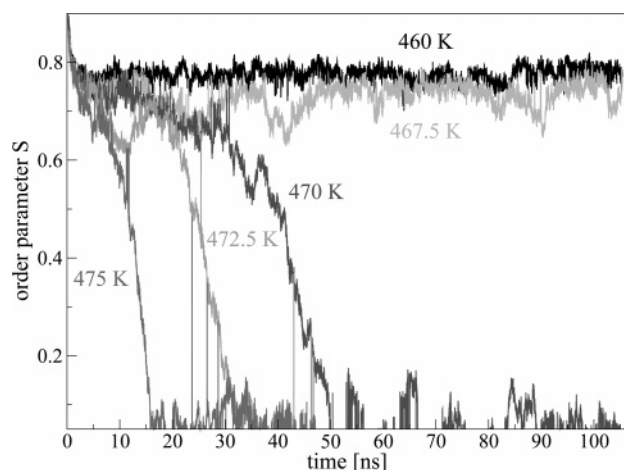
Atomistic Force Field for Azobenzene Compounds

J. Chem. Theory Comput., Vol. 3, No. 5, 2007 **1799**

Figure 13. Order parameter in the replica exchange simulations of 8AB8 (460−475 K). Each gray shade corresponds to one replica temperature as indicated in the graph (replicas at 462.5 and 465 K not displayed, they behave like the replica at 460 K). Exchanges between two replicas lead to the discontinuities in the order parameter due to the exchange of conformations. (The replicas at 475 and 472.5 K were discontinued after 48 ns of simulation time.)

range between 460 and 475 K were carried out as outlined in section 2.3. The temperature range had been determined beforehand by simulating the system at a number of different temperatures ranging from temperatures where the systems remains stable in the layered/ordered setup up to temperatures where the initial order quickly decays and one obtains an isotropic phase. The temperature shift of this range compared to the experimentally observed transition temperatures will be further addressed below. Figure 13 shows the order parameter eq 1 in the replica exchange simulations of 8AB8 in the temperature range from 460 to 475 K. Exchanges between replicas at different temperatures are observed which is visible as discontinuities in the order parameter due to the exchange of conformations. One nicely sees the loss of the original order in the replicas from 475 K down to 470 K (note that the replicas at 475 and 472.5 K were discontinued after 48 ns of simulation time). The remaining replicas below 470 K remain stable with an order parameter of ≈ 0.75.

Snapshots from these replica exchange simulations are shown in Figure 14. The left snapshot is taken from the replica at 470 K at a simulation time of 37 ns (order parameter $S \approx 0.6$), thus showing a structure during the transition from the layered setup to the isotropic state. The right snapshot is taken from the replica at 465 K at a simulation time of 86 ns ($S \approx 0.75$), showing a representative structure for the systems that remain stable in an ordered phase (the initial layered setup is still very well recognizable in this snapshot). In the left snapshot, which shows the system during the transition from smectic ordering to the isotropic state, one sees that at least partially the system does maintain some degree of order/alignment while the smectic layers are dissolving. The right snapshot shows the system at a lower temperature, and we can observe that, while the alignment along the *z*-direction is maintained, the layers start to dissolve, i.e., molecules move in the *z*-direction while they remain oriented. We also observe realignment of molecules

that had been lying between the layers perpendicular to the director.

The experimentally observed phases and transition temperatures cannot be fully reproduced with these classical atomistic simulations. The nematic phase (which would experimentally be expected between 372 and 385 K) is not observed, but the layered setup is stable up to a much higher temperature until it dissolves rapidly and the system goes directly to the isotropic phase (even though transient nematic-like structures are observed as well as molecules that leave the smectic layers and yet stay oriented). This phase behavior most likely has several reasons. First of all, the temperature range in which the nematic phase is observed experimentally for this compound is rather narrow (≈ 10 K), which is a challenge for computer simulations where overheating and finite size effects may play an important role and possibly lead to an overstabilization of the smectic layers. For example, an artificial stabilization of the smectic layers due to the anisotropic pressure scaling, which allows the aspect ratio of the sides of the orthorhombic box to adjust to the layered structure, cannot be ruled out and needs to be further investigated in the future. In addition, rather small variations in the classical force field may have large effects on the transition temperatures. Different factors can play a role in this context. For one, the intramolecular degrees of freedom determine the flexibility/stiffness of the individual molecules which plays an important role in the liquid−crystalline-phase behavior. In the first tests when the force field was parametrized we noticed that changes in the molecular flexibility have an effect on the thermal stability of the smectic phase (for instance we found that the transition temperature decreased after the azo group and the ether linkage between the azobenzene unit and the tails were reparametrized based on the all-QM simulations compared to first guesses made based on standard force field parameters for similar groups). A second important aspect concerning the force field are the intermolecular/nonbonded interactions. For 8AB8 the balance of aromatic/aromatic (azobenzene core), aliphatic/aliphatic (alkoxy tails) and aromatic/aliphatic interactions is particularly relevant (this menas that the liquid densities of the alkyl and aromatic fragments as well as the mixing properties of alkyl and aromatic groups have to be correctly reproduced). It should be noted that we are aware that there are procedures to optimize parameters for classical atomistic force fields for liquid−crystalline systems;[57−59] however, it was not our aim to provide an optimized classical force field for 8AB8 liquid crystals but to apply an existing force field (the GROMOS force field which is parametrized on thermodynamic properties in the liquid state) and to supplement the nonstandard parameters for the azo group. One key objective in the parametrization was the suitability of the classical model for further use in QM/MM simulations in order to study the influence of bulk liquid and anisotropic liquid−crystalline environments on the azobenzene photoisomerization. We also note that our set of bonded parameters for the azo group could be combined with a different nonbonded force field without having to reparametrize the AB unit itself.

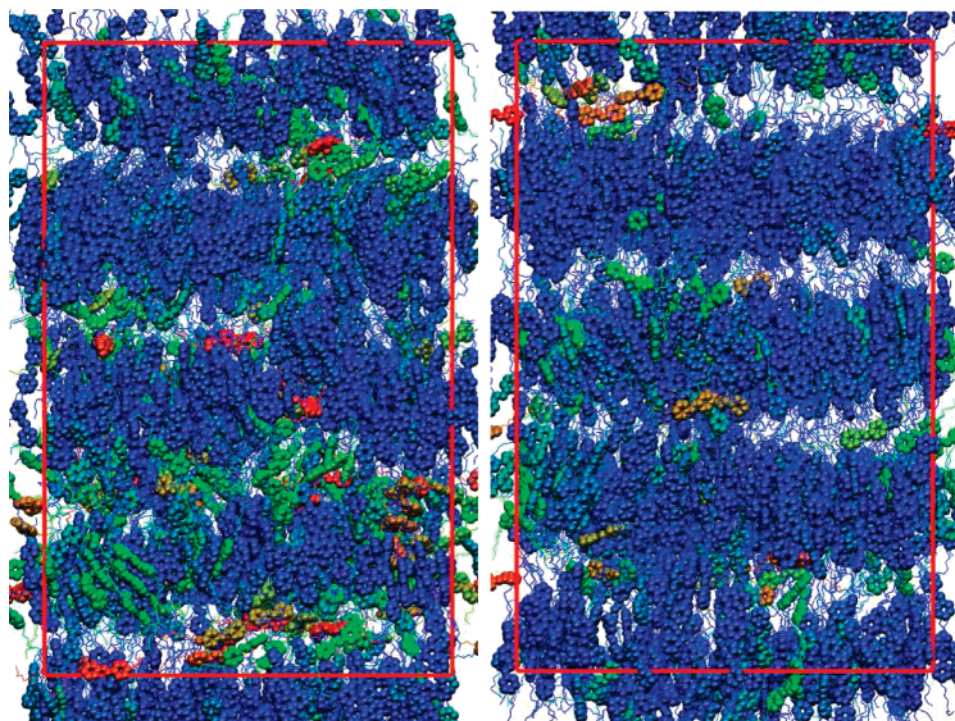We hope to get a better understanding of the phase behavior of 8AB8 in future multiscale simulations using

Figure 14. Snapshots from replica exchange simulations. The left snapshot stems from the replica at 470 K at a simulation time of 37 ns ($S \approx 0.6$), and the right snapshot stems from the replica at 465 K at a simulation time of 86 ns ($S \approx 0.75$). The red frame indicates the size of the periodic box. Spherical beads: azobenzene atoms, lines: alkoxy tails. The color shows the alignment of each molecule with respect to the director (from blue to red; blue: aligned along the director, i.e., along the *z*-direction; red: perpendicular to the director).

classical atomistic and coarse grained simulations. First simulations using a coarse grained (CG) model that was built on the classical atomistic one did indeed reproduce the nematic phase (a publication on the development of the CG model is in preparation). This CG model can be utilized to investigate systematically the phase behavior of 8AB8 and (after reintroduction of atomistic details into the CG coordinates, so-called inverse mapping) to obtain equilibrated atomistic coordinates. Since CG simulations lead to a significant speedup, we can also systematically study the influence of box size and shape on the relative stabilities of nematic and smectic phases and the resulting finite size effects—a comparison which due to the simulation time limitations would not be possible with all-atom simulations alone.

In order to characterize the ordered/smectic phase that is observed in the simulations we reorder the replicas to obtain trajectories which are continuous in conformation space which implies necessarily fluctuating temperatures. For these reordered replicas one can analyze diffusion constants in the *xy* planes and perpendicular to the layers along the *z*-direction. It is observed that in the case of the replicas that remain in the layered arrangement the in-plane diffusion is considerably faster than the diffusion perpendicular to the planes—characterizing the observed phase indeed as smectic and not as frozen.

In the following we study the influence of the anisotropic liquid−crystalline environment on the conformational distributions of the *trans*-AB functional units within the 8AB8 molecules. In order to compare with the conformations in pure liquid AB as discussed in the previous sections, the

liquid−crystalline system was quenched down to 400 K, both starting from a disordered/isotropic structure and from a layered/smectic structure. The resulting distributions are added to Figure 5a,c, and the distributions obtained from a vacuum simulation of 8AB8 were added as well for the sake of comparison. For all three simulations of 8AB8, the distribution of the phenyl−phenyl distance is narrower than in both gas-phase and liquid-phase *trans*-AB (see Figure 5a). This shows that the aliphatic tails have a sort of 'pulling influence' on the conformational equilibria of the AB core unit, again an effect which is potentially important for photoisomerization in condensed-phase environments such as liquid−crystalline materials. Figure 5c shows that the distribution functions of the CCNN dihedral angle, which measures the out-of-plane motions of the phenyl rings, in a single *trans*-8AB8 chain do not differ from *trans*-AB, whereas they are clearly affected in the two condensed-phase simulations of 8AB8. The distributions are narrower in the isotropic phase and even more so in the smectic phase, i.e., the oriented molecules are kept more planar due to the anisotropic environment.

Overall, our condensed-phase simulations show that there are various factors that very clearly influence the conformations of the AB photoactive functional unit compared to the noninteracting reference situation in the gas phase.

In particular, intramolecular effects due to the 'pulling' of the tails are observed in 8AB8, which are likely to play an important role in AB-containing photo(re)active materials in more general terms. In addition, intermolecular effects exist due to the bulk environment that are most pronounced in the case of an anisotropic liquid−crystalline environment.

Atomistic Force Field for Azobenzene Compounds

J. Chem. Theory Comput., Vol. 3, No. 5, 2007 **1801**

These results suggest that the condensed-phase environment may induce changes to the mechanism and efficiency of the photoisomerization which needs to be investigated in the future.

4. Conclusions and Outlook

In a long-term effort to being able to simulate photo(re)-active materials containing covalently bonded azobenzene (AB) functional units as photoswitches, we have extended and adapted a classical force field for AB based on ab initio molecular dynamics reference simulations and the GROMOS 45a3 force field. Using this novel force field we have presented a first application to the study of AB in the bulk liquid state. To this end, not only a standard purely classical molecular–mechanics (MM) setup but also a hybrid quantum-classical QM/MM approach, where only a single AB molecule has been treated quantum-mechanically (QM), has been used to conduct molecular dynamics simulations. Based on various observables we have verified that both levels of simulation yield conformational distributions that are consistent with each other. This agreement was an important initial goal of the effective parametrization in order to allow for smooth transitions between classical and quantum mechanical description of AB units in future adaptive multiscale simulations. This will be necessary to investigate the influence of bulk liquid and anisotropic liquid–crystalline environments on the photoisomerization mechanism of the AB functional group.

Furthermore, the AB force field has been extended to include aliphatic hydrocarbon chains that are connected via ether links to the phenyl rings. In particular, the extended azobenzene force field has been employed to study the liquid–crystalline azobenzene compound 8AB8. Using this force field the phase behavior of the liquid–crystalline AB compound 8AB8 has been studied by classical simulations using replica exchange techniques. The structures observed in these simulations give confidence that the experimental phases of 8AB8 can be described by the generated force field. However, in order to simulate time and length scales required to properly cover such phase transition processes and to systematically investigate the phase behavior of 8AB8, a coarser description of the system is necessary. The development of such a coarse grained model for 8AB8 based on the atomistic force field is on the way.

Apart from the above aspects of force field generation and validation we could also show that the liquid environment, and even more so the anisotropic environment in a liquid crystal, influences the conformational distributions of the *trans*-and *cis*-AB units as compared to the gas-phase reference at the same temperature. In particular, AB units in the cis arrangement are found to be much more affected by condensed-phase effects in comparison to the trans conformer. It is therefore essential for the study of photoisomer-izations of AB chromophores that are covalently embedded in materials to properly take into account environmental condensed-phase effects. Work along these directions is currently in progress.

References

(1) *Photoreactive organic thin films;* Sekkat, Z., Knoll, W., Eds.; Academic Press: San Diego, CA, 2002.

(2) *Molecular Switches;* Feringa, B. L., Ed.; Wiley-VCH: Weinheim, 2001.

(3) Stolow, A. *Ann. Rev. Phys. Chem.* **2003**, *54*, 89.

(4) Yesodha, S. K.; Pillai, C. K. S.; Tsutsumi, N. *Prog. Polym. Sci.* **2004**, *29*, 45.

(5) Yager, K. G.; Barrett, C. J. *J. Photochem. Photobiol., A* **2006**, *182*, 250.

(6) Nägele, T.; Hoche, R.; Zinth, W.; Wachtveitl, J. *Chem. Phys. Lett.* **1997**, *272*, 489.

(7) Fujino, T.; Arzhantsev, S. Y.; Tahara, T. *J. Phys. Chem. A* **2001**, *105*, 8123.

(8) Cembra, A.; Bernardi, F.; Garavelli, M.; Gagliardi, L.; Orlandi, G. *J. Am. Chem. Soc.* **2004**, *126*, 3234.

(9) Cattaneo, P.; Persico, M. *Phys. Chem. Chem. Phys.* **1999**, *1*, 4739.

(10) Ishikawa, T.; Noro, T.; Shoda, T. *J. Chem. Phys.* **2001**, *115*, 7503.

(11) Diau, W.-G. *J. Phys. Chem. A* **2004**, *108*, 950.

(12) Ciminelli, C.; Granucci, G.; Persico, M. *Chem. Eur. J.* **2004**, *10*, 2327.

(13) Schultz, T.; Quenneville, J.; Levine, B.; Toniolo, A.; Martinez, T. J.; Lochbrunner, S.; Schmitt, M.; Shaffer, J. P.; Zgierski, M. Z.; Stolow, A. *J. Am. Chem. Soc.* **2003**, *125*, 8098−8099.

(14) Tiago, M. L.; Ismail-Beigi, S.; Louie, S. G. *J. Chem. Phys.* **2005**, *122*, 094311.

(15) Toniolo, A.; Ciminelli, C.; Persico, M.; Martinez, T. *J. Chem. Phys.* **2005**, *123*, 234308.

(16) Crecca, C. R.; Roitberg, A. E. *J. Phys. Chem. A* **2006**, *110*, 8188−8203.

(17) Spörlein, S.; Carstens, H.; Satzger, H.; Renner, C.; Behrendt, R.; Moroder, L.; Tavan, P.; Zinth, W.; Wachtveitl, J. *Proc. Natl. Acad. Sci.* **2002**, *99*, 7998.

(18) Wachtveitl, J.; Spörlein, S.; Satzger, H.; Fonrobert, B.; Renner, C.; Behrendt, R.; Oesterhelt, D.; Moroder, L.; Zinth, W. *Biophys. J.* **2004**, *86*, 2350.

(19) Browne, W. R.; Feringa, B. L. *Nat. Nanotechnol.* **2006**, *1*, 25.

(20) Hugel, T.; Holland, N. B.; Cattani, A.; Moroder, L.; Seitz, M.; Gaub, H. E. *Science* **2002**, *296*, 1103.

(21) Kumar, G. S.; Neckers, D. C. *Chem. Rev.* **1989**, *89*, 1915−1925.

(22) Liu, Z. F.; Hashimoto, K.; Fujishima, A. *Nature* **1990**, *347*, 658.

(23) Sekkat, Z.; Dumont, M. *Appl. Phys. B* **1992**, *54*, 486.

(24) Ikeda, T.; Tsutsumi, O. *Science* **1995**, *268*, 1873.

(25) Hagen, R.; Bieringer, T. *Adv. Mater.* **2001**, *13*, 1805.

(26) Natansohn, A.; Rochon, P. *Chem. Rev.* **2002**, *102*, 4139−4175.

(27) Shibaev, V.; Bobrovsky, A.; Boiko, N. *Prog. Polym. Sci.* **2003**, *28*, 729−836.

(28) Yu, Y.; Nakano, M.; Ikeda, T. *Nature* **2003**, *425*, 145.

(29) Banerjee, I.; Yu, L.; Matsui, H. *J. Am. Chem. Soc.* **2003**, *125*, 9542.

(30) Tsutsumi, O.; Shiono, T.; Ikeda, T.; Galli, G. *J. Phys. Chem. B* **1997**, *101*, 1332−1337.

(31) Pieroni, O.; Fissi, A.; Angelini, N.; Lenci, F. *Acc. Chem. Res.* **2001**, *34*, 9.

(32) de Jeu, W. H. *J. Phys.* **1977**, *38*, 1265−1273.

(33) Car, R.; Parrinello, M. *Phys. Rev. Lett.* **1985**, *55*, 2471.

(34) Marx, D.; Hutter, J. Ab Initio Molecular Dynamics: Theory and Implementation. In *Modern Methods and Algorithms of Quantum Chemistry*; Grotendorst, J., Ed.; NIC: Jülich, 2000. www.theochem.rub.de/go/cprev.html (accessed June 2007).

(35) Hutter, J. et al. Car−Parrinello Molecular Dynamics: An *Ab Initio* Electronic Structure and Molecular Dynamics Program. www.cpmd.org (accessed June 2007).

(36) Perdew, J. P.; Burke, K.; Ernzerhof, M. *Phys. Rev. Lett.* **1996**, *77*, 3865.

(37) Perdew, J. P.; Burke, K.; Ernzerhof, M. *Phys. Rev. Lett.* **1997**, *78*, 1396.

(38) Martyna, G. J.; Klein, M. L.; Tuckerman, M. *J. Chem. Phys.* **1992**, *97*, 2635.

(39) Fukui, K.; Cline, J. I.; Frederick, J. H. *J. Chem. Phys.* **1997**, *107*, 4551−4563.

(40) Cox, S. R.; Kollman, P. A. *J. Comput. Chem.* **1984**, *5*, 129.

(41) Schuler, L. D.; Daura, X.; van Gunsteren, W. F. *J. Comput. Chem.* **2001**, *22*, 1205−1218.

(42) van Gunsteren, W. F.; Billeter, S. R.; Eising, A. A.; Hünenberger, P. H.; Krüger, P.; Mark, A. E.; Scott, W. R. P.; Tironi, I. G. *Biomolecular Simulation: The GROMOS96 Manual and User Guide*; Vdf Hochschulverlag AG an der ETH Zürich: Zürich, 1996.

(43) Scott, W. R. P.; Hünenberger, P. H.; Tironi, I. G.; Mark, A. E.; Billeter, S. R.; Fennen, J.; Torda, A. E.; Huber, T.; Krüger, P.; van Gunsteren, W. F. *J. Phys. Chem. A* **1999**, *103*, 3596−3607.

(44) Berendsen, H. J. C.; Postma, J. P. M.; van Gunsteren, W. F.; DiNola, A.; Haak, J. R. *J. Chem. Phys.* **1984**, *81*, 3684−3690.

(45) van der Spoel, D.; Lindahl, E.; Hess, B.; Groenhof, G.; Mark, A. E.; Berendsen, H. J. C. *J. Comput. Chem.* **2005**, *26*, 1701.

(46) Darden, T.; York, D.; Pedersen, L. *J. Chem. Phys.* **1993**, *98*, 10089−10092.

(47) Essmann, U.; Perera, L.; Berkowitz, M. L.; Darden, T.; Lee, H.; Pedersen, L. G. *J. Chem. Phys.* **1995**, *103*, 8577−8593.

(48) Hess, B.; Bekker, H.; Berendsen, H. J. C.; Fraaije, J. G. E. M. *J. Comput. Chem.* **1997**, *18*, 1463−1472.

(49) Sugita, Y.; Okamoto, Y. *Chem. Phys. Lett.* **1999**, *314*, 141−151.

(50) Laio, A.; VandeVondele, J.; Rothlisberger, U. *J. Chem. Phys.* **2002**, *116*, 6941.

(51) Carloni, P.; Rothlisberger, U.; Parrinello, M. *Acc. Chem. Res.* **2002**, *35*, 455−464.

(52) Wilson, E. B., Jr.; Decius, J. C.; Cross, P. C. *Molecular Vibrations*; McGraw-Hill: New York, 1955.

(53) Adamson, A. W.; Vogler, A.; Kunkely, H.; Wachter, R. *J. Am. Chem. Soc.* **1978**, *100*, 1300.

(54) Tsuji, T.; Takashima, H.; Takeuchi, H.; Egawa, T.; Konaka, S. *J. Phys. Chem. A* **2001**, *105*, 9347.

(55) Bayly, C. I.; Cieplak, P.; Cornell, W.; Kollman, P. A. *J. Phys. Chem.* **1993**, *97*, 10269.

(56) Case, D. A.; Pearlman, D. A.; Caldwell, J. W.; Cheatham, T. E., III; Wang, J.; Ross, W. S.; Simmerling, C. L.; Darden, T. A.; Merz, K. M.; Stanton, R. V.; Cheng, A. L.; Vincent, J. J.; Crowley, M.; Tsui, V.; Gohlke, H.; Radmer, R. J.; Duan, Y.; Pitera, J.; Massova, I.; Seibel, G. L.; Singh, U. C.; Weiner, P. K.; Kollman, P. A. *AMBER 7*; University of California: San Francisco, CA, 2002.

(57) Cheung, D. L.; Clark, S. J.; Wilson, M. R. *Phys. Rev. E* **2002**, *65*, 051709.

(58) Wilson, M. R. *Int. Rev. Phys. Chem.* **2005**, *24*, 421−455.

(59) Bizzarri, M.; Cacelli, I.; Prampolini, G.; Tani, A. *J. Phys. Chem. A* **2004**, *108*, 10336−10341.

(60) Fliegl, H.; Köhn, A.; Hättig, C.; Ahlrichs, R. *J. Am. Chem. Soc.* **2003**, *125*, 9821.

(61) Bouwstra, J. A.; Schouten, A.; Kroon, J. *Acta Crystallogr., Sect. C: Cryst. Struct. Commun.* **1983**, *39*, 1121.

(62) Traetterberg, M.; Hilmo, I.; Hagen, K. *J. Mol. Struct.* **1977**, *39*, 231.

(63) Mostad, A.; Romming, C. *Acta Chem. Scand.* **1971**, *25*, 3561.

(64) Schulze, F. W.; Petrick, H.-J.; Cammenga, H. K.; Klinge, H. *Z. Phys. Chem. (Munich)* **1977**, *107*, 1.